Impact of East Asian Winter and Australian Summer Monsoons on the Enhanced Surface Westerlies over the Western Tropical Pacific Ocean Preceding the El Niño Onset

YANGXING ZHENG

Center for Ocean–Atmospheric Prediction Studies, The Florida State University, Tallahassee, Florida

RENHE ZHANG

State Key Laboratory of Severe Weather (LaSW), Chinese Academy of Meteorological Sciences, Beijing, China

MARK A. BOURASSA

Center for Ocean–Atmospheric Prediction Studies, and Department of Earth, Ocean and Atmospheric Science, The Florida State University, Tallahassee, Florida

(Manuscript received 26 June 2013, in final form 18 October 2013)

ABSTRACT

Composite analysis from NCEP–NCAR reanalysis datasets over the period 1948–2007 indicates that stronger East Asian winter monsoons (EAWM) and stronger Australian summer monsoons (ASM) generally coexist in boreal winters preceding the onset of El Niño, although the EAWM tend to be weak after 1990, probably because of the decadal shift of EAWM and the change in El Niño events from cold-tongue type to warm-pool type. The anomalous EAWM and ASM enhance surface westerlies over the western tropical Pacific Ocean (WTP). It is proposed that the enhanced surface westerlies over the WTP prior to El Niño onset are generally associated with the concurrent anomalous EAWM and ASM. A simple analytical atmospheric model is constructed to test the hypothesis that the emergence of enhanced surface westerlies over the WTP can be linked to concurrent EAWM and ASM anomalies. Model results indicate that, when anomalous northerlies from the EAWM converge with anomalous southerlies from the ASM, westerly anomalies over the WTP are enhanced. This result provides a possible explanation of the co-impact of the EAWM and the ASM on the onset of El Niño through enhancing the surface westerly over the WTP.

1. Introduction

Episodes of strong westerly winds over the western tropical Pacific Ocean (WTP) occur mostly before El Niño events. Westerly wind bursts (WWBs) are such westerly winds of high frequency (<90 days). WWBs typically last 6–20 days, have maximum wind speeds of 8–20 $m\,s^{-1}$ (Harrison and Vecchi 1997), and occur 0–8 times per year (Verbickas 1998). WWBs play an important role in the generation of surface westerly anomalies preceding El Niño events. Researchers have proposed various mechanisms as explanations for the generation of WWBs. Early studies (Lim and Chang 1981; Love 1985a,b; Chu 1988; Li 1990; Compo et al. 1999) suggest that a cold surge from the extratropics associated with an anomalous East Asian winter monsoon (EAWM) is one important mechanism for the generation of WWBs. The generation of WWBs also may be associated with twin or individual tropical cyclones (Keen 1982, 1988), the passage of the convective events on the MJO (30–70 days; Lau et al. 1989; Gutzler 1991; Sui and Lau 1992; Hendon and Liebmann 1994; Hendon et al. 1998), sub-MJO time scales (6–30 days; Kiladis and Loon 1988; Kiladis et al. 1994), or a combination of these phenomena (Yu and Rienecher 1998). In the literature, these high-frequency fluctuations are believed to be closely associated with the onset of an El Niño event. However, many studies also suggest that the

Corresponding author address: Yangxing Zheng, Center for Ocean–Atmospheric Prediction Studies, The Florida State University, 2000 Levy Avenue, Room 238, Building A, Tallahassee, FL 32306.
E-mail: yzheng@fsu.edu

DOI: 10.1175/JCLI-D-13-00369.1

variation of surface winds over the WTP on the interannual time scale plays an important role in the occurrence of El Niño events (e.g., Rasmusson and Carpenter 1982; Zhang and Huang 1998; Huang et al. 1998; Rong et al. 2011). The westerly anomalies over the WTP can generate downwelling Kelvin waves that propagate eastward and cause warming in the eastern equatorial Pacific Ocean (Huang et al. 1998). In this study, we focus on the genesis of low-frequency (more than 90 days but less than 6 months) westerly anomalies preceding the onset of El Niño.

The genesis of westerly anomalies over the WTP is postulated to be involved in various monsoon systems. In an observational study, Xu and Chan (2001) suggested that the enhancement of westerly anomalies associated with El Niño events over the WTP is influenced not only by the East Asian monsoon but also by the Australian monsoon, emphasizing the role of the southerly anomalies associated with the transition of the Australian monsoon. Zhang et al. (2001) also showed that anomalous southerly winds appear prior to the SST increase in the eastern equatorial Pacific Ocean. However, neither the physical process of southerly wind formation nor the process by which the East Asian and Australian monsoons affect westerly anomalies over the WTP has been clear. This work provides a potential explanation: the anomalous EAWM associated with anomalous cooling over East Asia and the Australian summer monsoon (ASM) associated with anomalous warming over Australia can lead to the generation of enhanced surface westerlies over the WTP. Therefore, westerly anomalies over the WTP are relevant to the anomalous ASM and EAWM system. Indeed, enhancement of westerly anomalies over the WTP associated with such anomalous thermal forcing appears in a simple, linear, Gill-type analytic atmospheric model. The major purpose of this short work is to examine the genesis of westerly anomalies over the WTP and its potential dynamical link to anomalous EAWM and ASM features for the enhancement of surface westerlies.

2. Data

The present study uses datasets from two sources. Monthly-mean global sea surface temperature (SST) data on a 2° latitude by 2° longitude global grid for the period January 1948–December 2007 are taken from the National Oceanic and Atmospheric Administration extended reconstructed version 3 (NOAA ER V3) SST (Xue et al. 2003; Smith et al. 2008). These data, which include the most recently available International Comprehensive Ocean–Atmosphere Data Set (ICOADS) release 2.4, were optimally generated by improved statistical methods that allow a stable reconstruction using sparse data. Monthly-mean global zonal and meridional surface wind components, surface air temperatures, and surface air pressure on a 2.5° latitude by 2.5° longitude grid for the period January 1948–December 2007 are taken from the National Centers for Environmental Prediction–National Center for Atmospheric Research (NCEP–NCAR) Reanalysis 1 product (Kalnay et al. 1996).

3. Association of surface westerlies over WTP with EAWM and ASM

In this section, observational features of WTP surface westerlies as well as the features of East Asian and Australian monsoons in boreal winters preceding an El Niño onset are examined and compared with these features in boreal winters of the other years. The association of WTP westerlies with East Asian–Australian monsoons in boreal winters prior to an El Niño onset is first investigated using a composite analysis. A composite approach is used with the underlying assumption that the dominant features of the samples behave in a similar manner and are governed by the same mechanism. Of course, it is very unlikely that all samples/events behave in the same/similar manner and that they occur because of the same mechanism, but the composite approach is adopted as a first means of identifying the dominant features that potentially behave in a similar manner and are governed by the same mechanism. The underlying assumption regarding a composite will be examined using a conditional probability analysis. In this study, an El Niño episode is said to occur if a 3-month running mean of sea surface temperature anomalies (SSTAs) in the Niño-3.4 region (5°S–5°N, 170°–120°W) (i.e., Niño-3.4 index) exceeds a +0.5°C threshold for at least five consecutive months. Following this definition and using data from NOAA ER V3 SST, we identify 16 individual El Niño events during the period January 1948–December 2007. These 16 El Niño events, the starting and ending month for each, and the duration in months of each event are listed in Table 1.

The annual mean and annual cycle of monthly-mean data are computed first on the basis of the January 1948–December 2007 monthly-mean data described in section 2. The annual mean and annual cycle are then removed to obtain the anomalies; thus, the impacts of background and seasonality on analysis are ruled out, assuming that the background and the seasonality do not shift over time. Figure 1 shows the anomalous observed surface atmospheric features averaged over boreal winters (November–April) prior to the onset of the 16 El Niño events. Figure 1a presents the surface air

TABLE 1. El Niño episodes over the period 1948–2007 as defined by a 3-month running mean of SST anomalies in the Niño-3.4 region (5°S–5°N, 170°–120°W) and exceeding a +0.5°C threshold for at least five consecutive months. The anomalies are derived from the 1948–2007 SST climatology.

Begin	End	Duration (months)
Jun 1951	Dec 1951	7
Apr 1957	Jul 1958	16
May 1963	Dec 1963	8
May 1965	Mar 1966	11
Jun 1968	Jan 1970	20
Apr 1972	Feb 1973	11
Aug 1976	Jan 1977	6
May 1977	Jan 1978	9
Apr 1982	Jul 1983	16
Jul 1986	Jan 1988	19
Apr 1991	Jul 1992	16
Apr 1994	Feb 1995	11
Apr 1997	May 1998	14
Apr 2002	Feb 2003	11
May 2004	Jan 2005	9
May 2006	Jan 2007	9

temperature anomalies during these boreal winters. A dominant anomalous surface cooling over the Eurasian continent and an anomalous surface warming over Australia reflect an intensification of the land–sea thermal contrast. Since the fundamental mechanism of the monsoons is land–sea thermal contrast (Webster 1987), an anomalous surface cooling over the Eurasian continent favors an anomalous EAWM and an anomalous warming relative to its surrounding seas favors an anomalous ASM. Meanwhile, there is an anomalous surface high pressure with horizontal divergence of surface winds over the East Asia region (15°–40°N, 100°–130°E) and a weak anomalous low pressure with horizontal convergence of surface winds over Australia (Fig. 1b). Figure 1c illustrates the composite evolution of the Niño-3.4 index, the surface westerly anomaly (WA), the EAWM, and the ASM anomalies prior to the onset of these 16 El Niño events. Here a westerly anomaly is defined as the anomalous surface zonal winds averaged over 10°S–10°N, 110°–160°E since westerly anomalies generally occur in this region. The EAWM is defined as the meridional surface winds averaged over 20°–40°N, 110°–130°E and the ASM is defined as the meridional surface winds averaged over 30°–10°S, 100°–120°E. Note that the sign of the EAWM is reversed so that the northerly anomaly is positive. El Niño (−1) and El Niño (0) represent the years preceding and the years of El Niño episodes, respectively. It is evident that westerly anomalies start around October of El Niño (−1) and evolve through August of El Niño (0), accompanied by anomalous northerlies and southerlies from the EAWM

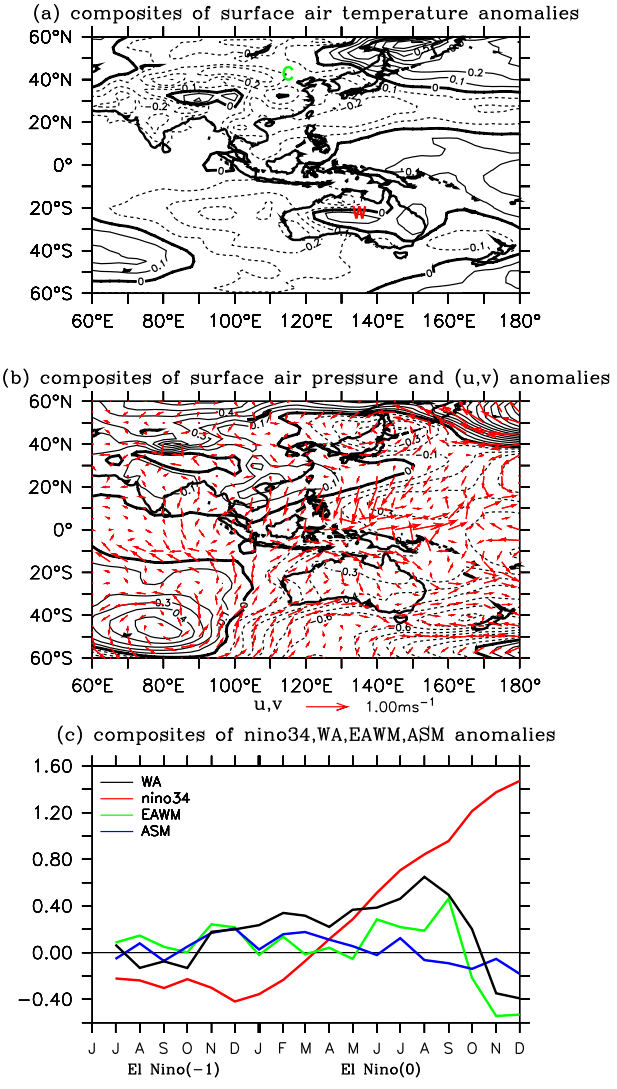

FIG. 1. Boreal winter (November–April) composites of (a) surface temperature anomalies (black contours, °C); (b) surface air pressure (black contours, hPa) and surface wind vector anomalies (red vectors, m s^{-1}); and (c) evolution of composite Niño-3.4 index (red line, °C) and westerly (black), EAWM (green), and ASM (blue) anomalies (m s^{-1}) preceding 16 El Niño episodes during the period 1948–2007. The sign of EAWM is reversed so that the northerly anomaly is positive. The major warm (cold) region is denoted by a red W (green C) in (a).

and the ASM, respectively. Here the results from composite analysis indicate that the EAWM and the ASM appear almost concurrently prior to the onset of El Niño, accompanied by westerly anomalies over the western tropical Pacific Ocean, indicating that both northerly anomalies in the East Asian monsoon zone and southerly anomalies in the Australian monsoon zone may play a role in the westerly anomalies over the WTP.

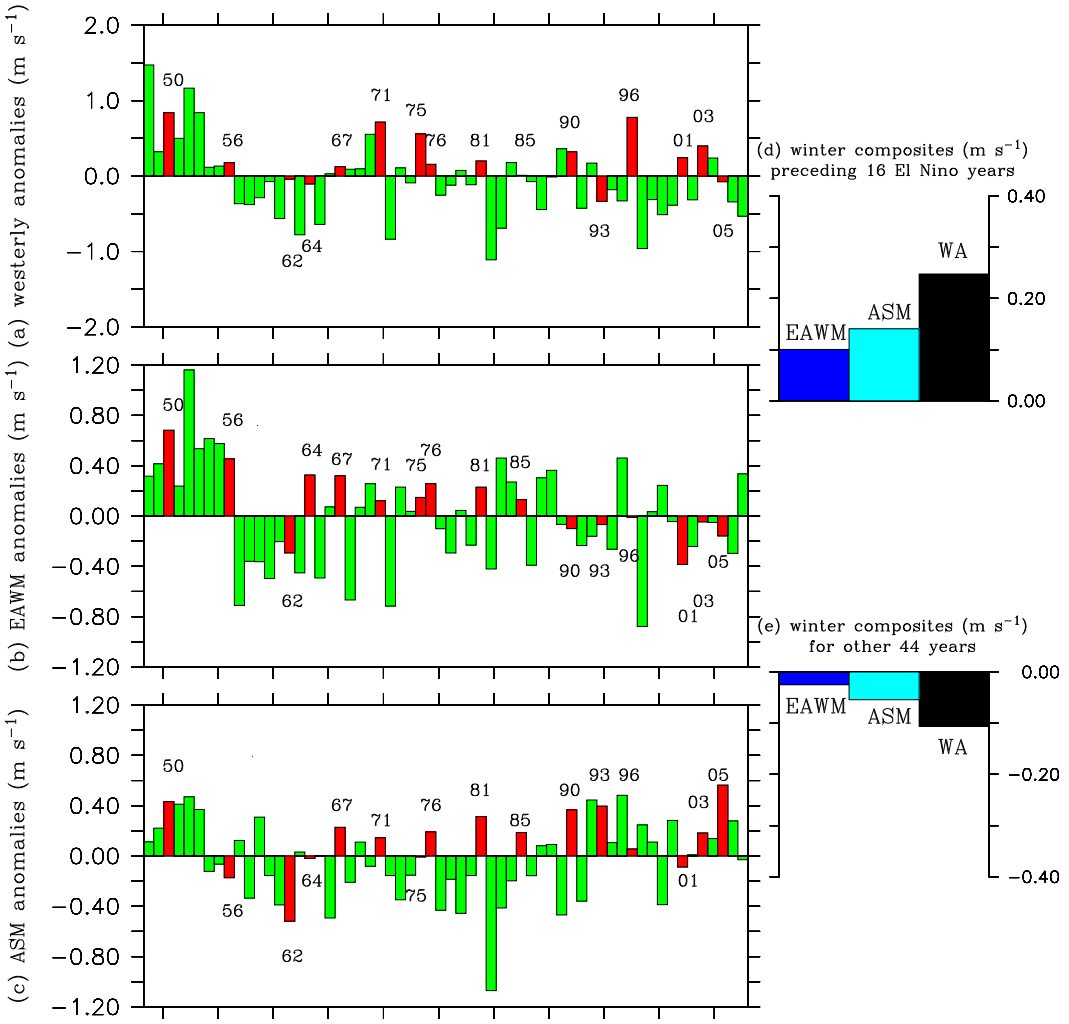

FIG. 2. (a) Westerly anomalies, (b) EAWM anomalies, and (c) ASM anomalies ($m\,s^{-1}$) averaged over boreal winter (November–April) during the period 1948–2007. The sign of EAWM is reversed so that the northerly anomaly is positive. In (a)–(c), westerly, EAWM, and ASM anomalies preceding the 16 El Niño episodes are denoted by red bars; the number of winter years are included at the top or bottom of the bars. WA, EAWM, and ASM anomalies in the 44 non–El Niño (−1) winters are denoted by green bars. Also shown are composites of westerly (black), EAWM (blue), and ASM (cyan) anomalies based on (d) the 16 El Niño (−1) winters and (e) the 44 non–El Niño (−1) winters during the period 1948–2007.

To see whether the WTP westerly anomalies are closely tied to the anomalous EAWM and ASM, the zero-lag correlation coefficients between the WTP westerly anomalies and both the EAWM and the ASM anomalies averaged over the boreal winters (November–April) are calculated. Zero-lag correlation coefficients between the WTP westerly anomalies and the EAWM (i.e., 0.55) and between the WTP westerly anomalies and the ASM (i.e., 0.36) are calculated. Both are larger than the critical correlation coefficient (i.e., 0.25) and thus are significant at a 95% confidence level. Therefore, the boreal winter WTP westerly anomalies are closely associated with the anomalies of both the EAWM and the ASM. However, features of the EAWM and/or the ASM may be critically different between the El Niño (−1) winters and the non–El Niño (−1) winters [i.e., other than El Niño (−1) winters], consequently exerting a different influence on the westerly anomalies. Figures 2a–c show the boreal winter-averaged (November–April) westerly anomalies and EAWM and ASM anomalies for the years 1948–2007. A positive westerly anomaly is present in 12 of 16 El Niño (−1) winters. The positive westerly anomalies also appear in 17 of the 44 non–El Niño (−1) winters. Therefore, when an El Niño event occurs, there is a 75% probability (12/16) that a positive westerly anomaly is present

prior to its onset. In the non–El Niño (−1) winters, there is a 39% probability (17/44) that a positive westerly anomaly is present. As a result, if an El Niño event has been triggered, the positive westerly anomaly is usually found in the preceding winter. Figures 2d,e indicate the composite relationship between the winter-averaged westerly anomalies and the EAWM and ASM anomalies in the 16 El Niño (−1) winters and in the 44 non–El Niño (−1) winters, respectively. Overall, the presence of a positive westerly anomaly in an El Niño (−1) winter is generally accompanied by the coexistence of a positive EAWM anomaly and a positive ASM anomaly. In the 44 non–El Niño (−1) winters, the presence of an easterly anomaly is generally accompanied by a weak negative EAWM anomaly and a weak negative ASM anomaly. It should be pointed out that among these 44 non–El Niño (−1) winters, such as 1948, 1949, 1951, 1952, and 1953, the positive westerly anomalies are also present and are accompanied by a positive EAWM anomaly and a positive ASM anomaly. Such cases are not dominant in non–El Niño (−1) boreal winters during 1948–2007, however.

It is reasonable to ask whether the features of the EAWM and the ASM in El Niño (−1) winters are significantly different from those in non–El Niño (−1) winters during which a positive westerly anomaly similarly appears. Therefore, the features of the EAWM and the ASM during El Niño (−1) winters are examined and compared to those features during non–El Niño (−1) winters during which a positive westerly anomaly occurs. The EAWM and the ASM anomalies and the westerly anomalies in the two types of winters during the period of 1953–2007 are shown in Fig. 3. During the period of 1953–2007, a positive westerly anomaly appears during 11 El Niño (−1) winters and 13 non–El Niño (−1) winters. On one hand, positive EAWM anomalies are predominantly present in both El Niño (−1) winters (64% probability or 7/11) and in non–El Niño (−1) winters (about 69% probability or 9/13) during which a positive westerly anomaly is simultaneously present (Fig. 3b). On the other hand, strong positive ASM anomalies are predominantly present in El Niño (−1) winters (about 73% probability or 8/11) and are not often present in non–El Niño (−1) winters (about 31% probability or 4/13) during which a positive westerly anomaly is simultaneously present. The conditional probability analysis clearly illustrates that, when a westerly anomaly occurs in boreal winter prior to an El Niño onset, it is most often accompanied by a positive ASM anomaly (i.e., anomalous southerly) and a positive EAWM anomaly (i.e., anomalous northerly). The strong EAWM anomalies (i.e., anomalous northerlies) alone may not necessarily indicate the onset of an El Niño event in the following year. This can also be seen in the composite analysis shown in Fig. 3d. Note that westerly anomalies are generally strengthened in El Niño (−1) winters relative to non–El Niño (−1) winters (Figs. 3a,d). Note that the data of 1948–52 are not included for composite analysis owing to the extremely large values of positive westerly anomalies in the boreal winters of 1948 and 1952 relative to other non–El Niño (−1) winters (Fig. 2a) when positive westerly anomalies were present. Inclusion of the two extremely large values for 1948 and 1952 in the composite analysis would undermine the contribution to amplitude in the westerly anomalies from other non–El Niño (−1) winters. To better demonstrate that the surface westerly anomalies in most non–El Niño (−1) winters during which a positive westerly anomaly was present are generally much weaker than those in El Niño (−1) winters during 1948–2007, we exclude the data of the first five years for composite analysis.

Table 2 demonstrates the El Niño (−1) years and the probability of occurrence of different anomalous EAWM and ASM features during which a positive westerly anomaly occurred in El Niño (−1) winters for the period 1948–2007. The probability that a strong EAWM and a strong ASM coexist, mostly prior to 1990, is 50%, which equals the total of the other three classifications. As seen in Table 2, a strong EAWM and a strong ASM sometimes do not coexist in El Niño (−1) winters; a weak EAWM (i.e., a southerly anomaly) coexists with a positive westerly anomaly after 1990. To understand why a weak EAWM can coexist with a positive westerly anomaly, we further examine the atmospheric features on the basis of the composite analysis for 1990, 1996, 2001, and 2003 (Fig. 4). Figure 4 clearly indicates that the WTP westerly anomaly is not directly attributed to the EAWM, but that it is primarily associated with atmospheric circulation over the tropical western–central Pacific Ocean (Fig. 4b), where an anomalous surface warming dominates (Fig. 4a). The appearance of a negative EAWM anomaly after 1990 may arise from the decadal shift of the EAWM in the late 1980s (Wang et al. 2009), which is associated with anomalous surface warming in winters over the Eurasian continent (Fig. 4a).

It has been reported (Larkin and Harrison 2005a,b; Ashok et al. 2007; Kao and Yu 2009; Kug et al. 2009) that the warm-pool (WP) El Niño events with major SSTA centered in the central Pacific Ocean near the edge of the warm pool mostly occurred in the early 1990s and 2000s; the cold-tongue (CT) El Niño events with major SSTA positioned over the eastern Pacific Ocean mostly occurred before 1990. The WP El Niño events occurred after 1990 when the tropical Pacific decadal variability (PDV) was in warm phases. We speculate that the phase

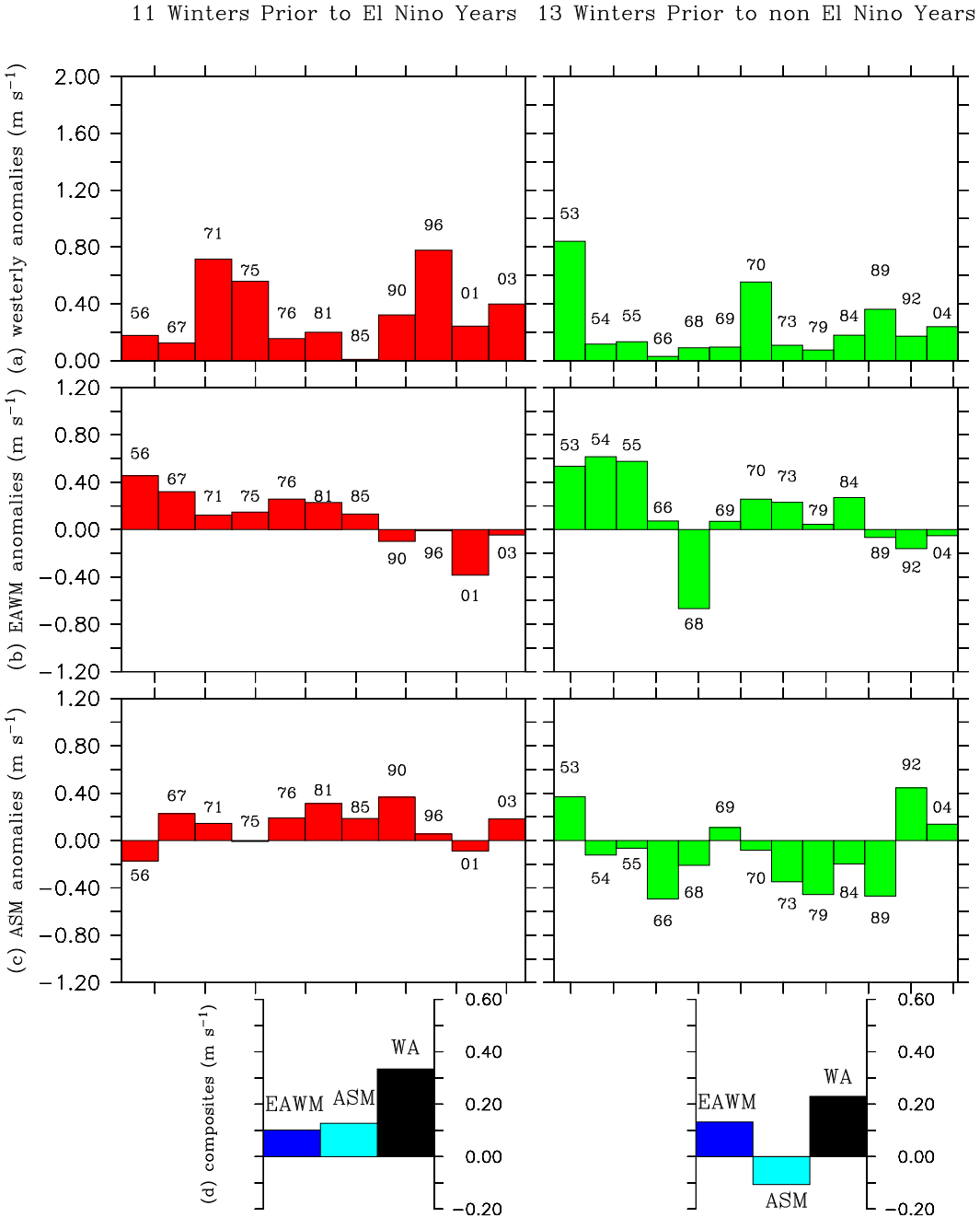

FIG. 3. (a) Westerly anomalies, (b) EAWM anomalies, and (c) ASM anomalies (in m s^{-1}) in (left) 11 El Niño (−1) boreal winters (red bars) and (right) 13 non–El Niño (−1) boreal winters (green bars) in which a positive winter-averaged (November–April) westerly anomaly was present during 1953–2007. The years of winter are denoted at the top or bottom of the bars in (a)–(c). (d) Composites of westerly (black), EAWM (blue), and ASM (cyan) anomalies based on the 11 El Niño (−1) boreal winters and based on the 13 non–El Niño (−1) boreal winters as described in (a)–(c).

shift of the PDV may be partly responsible for the weak EAWM after 1990. Thus, when the EAWM is weak, it may not contribute to the westerly anomalies over the WTP after 1990. Nevertheless, the relationship of a stronger EAWM to a westerly anomaly is robust, which is revealed by the statistical observational analyses. Our major conclusion is that the coexistence of stronger EAWM and ASM during El Niño (−1) winters

TABLE 2. El Niño (−1) winters of anomalous EAWM and ASM features during which a positive WA occurs for the period 1948–2007 and probability of occurrence in four cases. The + (−) sign in parentheses denotes a positive (negative) anomaly of the EAWM and the ASM.

	EAWM (+) and ASM (+)	EAWM (+) and ASM (−)	EAWM (−) and ASM (+)	EAWM (−) and ASM (−)
El Niño (−1) winters	1950, 1967, 1971, 1976, 1981, 1985	1956, 1975	1990, 1996, 2003	2001
Probability	50%	16.7%	25%	8.3%

is closely related to the advent of stronger westerly anomalies over the WTP. Our conclusion is not contradicted by the lack of the coexistence between EAWM and ASM after 1990 since our conclusion is based on a composite analysis of a 60-yr record (Figs. 1c, 2d, and 3d), not on individual events.

The above observational analysis clearly shows that the area-averaged time-mean westerly anomalies over the WTP associated with ASM are significantly different in El Niño (−1) winters and in non–El Niño (−1) winters. The prominent coexistence of strong EAWM and ASM anomalies favors an enhanced westerly anomaly in association with an El Niño onset in the following year. A strong EAWM anomaly alone can produce a positive westerly anomaly over the WTP, but it may not trigger an El Niño event in the following year.

We hypothesize that the distribution of surface temperature anomalies shown in Fig. 1a may be responsible for the coexistent northerly anomalies in the EAWM zone and the southerly anomalies in the ASM zone. When both EAWM and ASM are strong, the westerly anomalies are enhanced over the WTP; a strong EAWM alone may produce only weak westerly anomalies. This hypothesis is tested in a Gill-type analytical atmospheric model, which is discussed in the following section.

4. Dynamical role of EAWM and ASM in surface westerlies over the WTP

A typical thermal feature of strong anomalous EAWM and ASM is an anomalous cooling over the Eurasian continent and an anomalous warming over Australia relative to the surrounding seas (i.e., strong land–sea thermal contrast) as shown in Fig. 1a. The Gill-type model provides an atmospheric response for a given steady-state, idealized diabatic forcing: an anomalous cooling over the Eurasian continent and an anomalous warming over Australia similar to that shown in Fig. 1a. For clarity and completeness, the analytical solutions of the models are derived.

a. Model and solutions

The basic model is described by the following equations:

$$\varepsilon u - \frac{1}{2} y v + \frac{\partial \phi}{\partial x} = 0, \tag{1a}$$

$$\frac{1}{2} y u + \frac{\partial \phi}{\partial y} = 0, \tag{1b}$$

and

$$\left(\frac{\partial u}{\partial x} + \frac{\partial v}{\partial y}\right) + \varepsilon \phi = Q, \tag{1c}$$

where u and v are the perturbations of low-level zonal and meridional winds, respectively. Other variables and parameters are defined as follows: ϕ is the geopotential height perturbation; ε is both the Rayleigh friction coefficient and the Newtonian cooling coefficient; and Q is the forcing (i.e., diabatic heating/cooling rate) whereas a negative Q implies heating. The basic model described by (1a)–(1c) was first introduced by Matsuno (1966) and has been known as the Gill model since Gill (1980) first used it to examine the atmospheric response to the prescribed diabatic heating generally located near the equator. The forcing location in this study is different from Gill's (1980) because we impose the forcing in the midlatitude region. In fact, the Gill model has been used by previous studies in investigating the dynamic response of the tropical atmosphere to midlatitude forcing (e.g., Lim and Chang 1981; Lau and Lim 1982). It has also been widely used in ENSO studies (e.g., Cane and Zebiak 1985; Cane et al. 1986; Battisti 1988; Battisti and Hirst 1989).

To solve the system, we use the Gill (1980) method. We first introduce two new nondimensional variables that are defined by

$$\Psi = \phi + u \tag{2a}$$

and

$$\mathrm{X} = \phi - u. \tag{2b}$$

Through some simple substitutions, the system (1a)–(1c) is changed into

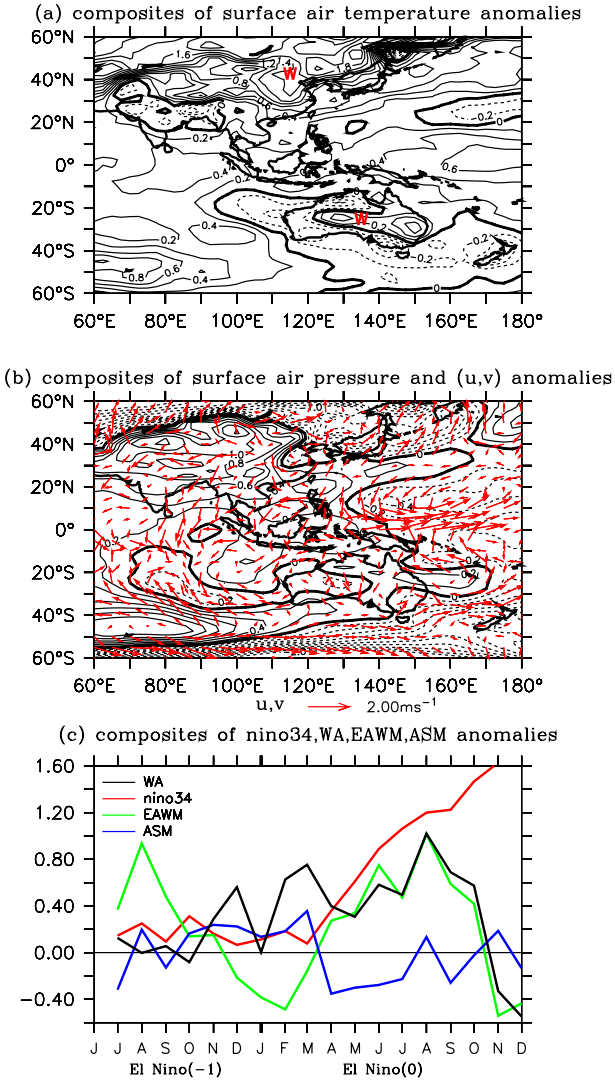

FIG. 4. As in Fig. 1, but based on 4 El Niño (−1) winters after 1990 (1990, 1996, 2001, and 2003) during which strong EAWM and ASM do not coexist. The warm centers are denoted by a red W over the Asian and Australian continents in (a).

$$\varepsilon\Psi + \frac{\partial\Psi}{\partial x} + \frac{\partial v}{\partial y} - \frac{1}{2}yv = Q, \tag{3a}$$

$$\varepsilon X + \frac{\partial X}{\partial x} + \frac{\partial v}{\partial y} + \frac{1}{2}yv = Q, \tag{3b}$$

and

$$\frac{\partial\Psi}{\partial y} + \frac{1}{2}y\Psi + \frac{\partial X}{\partial y} - \frac{1}{2}yX = 0. \tag{3c}$$

Since the free solution of the system (3a)–(3c) has the form of a parabolic cylinder function $D_n(y)$, where $D_n(y) = (-1)^n \exp(y^2/4)(d^n/dy^n)\exp(-y^2/2)$, the solutions for the specified forcing can be found by expanding the variables Ψ, X, v, and Q in terms of these functions,

$$(\Psi, X, v, Q)(x,y) = \sum_{n=0}^{\infty} (\Psi_n, X_n, v_n, Q_n)(x)D_n(y). \tag{4}$$

By substituting (4) into (3a)–(3c), we obtain

$$\frac{\partial\Psi_0}{\partial x} + \varepsilon\Psi_0 = Q_0, \tag{5a}$$

$$X_{n-1} = (n+1)\Psi_{n+1}, \quad (n = 1,2,3,\ldots), \tag{5b}$$

$$\left(-\frac{1}{2n+1}\right)\frac{\partial\Psi_{n+1}}{\partial x} + \varepsilon\Psi_{n+1} = \frac{nQ_{n+1} + Q_{n-1}}{2n+1}, \quad (n = 1,2,3,\ldots), \tag{5c}$$

$$\Psi_1 = 0, \tag{5d}$$

$$v_0 = -Q_1, \tag{5e}$$

and

$$v_n = \frac{2(n+1)}{2n+1}\frac{\partial\Psi_{n+1}}{\partial x} - \frac{(n+1)Q_{n+1} - Q_{n-1}}{2n+1}, \quad (n = 1,2,3,\ldots). \tag{5f}$$

Equation (5a) represents eastward propagation of a Kelvin wave with unit phase speed, and (5c) represents the westward propagation of Rossby waves with a phase speed of $-c_n$ ($c_n = 1/2n+1$).

In this study, we examine the steady-state atmospheric response to the given idealized forcing located near the midlatitudes. Therefore, we assume that the forcing has the form of

$$Q(x,y) = A\exp[-\lambda^2(y-y_c)^2 - \alpha^2(x-x_c)^2] = \sum_{n=0}^{\infty} Q_n(x)D_n(y), \tag{6}$$

where A is the amplitude of the forcing and the cooling (heating) rate if A is positive (negative); (x_c, y_c) is the center of cooling/heating source; and λ^{-1} is the length scale of Gaussian function in the y direction. The term $Q_n(x)$ is defined by

$$Q_n(x) = q_n\exp[-\alpha^2(x-x_c)^2], \tag{7}$$

where $1/\alpha$ represents the length scale of heat function (i.e., forcing) in the longitudinal direction.

The solution for (5a) and (5c) under the forcing of (7) can be easily obtained by

$$\Psi_0 = q_0 \exp[-\varepsilon(x - x_c)] \frac{\sqrt{\pi} \exp\left(\frac{\varepsilon}{2\alpha}\right)^2}{2\alpha} \times \mathrm{Erfc}\left[\frac{\varepsilon}{2\alpha} - \alpha(x - x_c)\right] \quad (8)$$

and

$$\Psi_{n+1} = (nq_{n+1} + q_{n-1}) \exp\left[-\frac{\varepsilon(x - x_c)}{-c_n}\right] \times \frac{\sqrt{\pi} \exp\left[\frac{\varepsilon}{2\alpha(-c_n)}\right]^2}{2\alpha} \mathrm{Erfc}\left[\alpha(x - x_c) - \frac{\varepsilon}{2\alpha(-c_n)}\right], \quad (n = 1, 2, 3, \ldots), \quad (9)$$

where $\mathrm{Erfc}(z)$ is the complementary error function, which is defined by

$$\mathrm{Erfc}(z) = \frac{2}{\sqrt{\pi}} \int_z^\infty \exp(-t^2)\, dt. \quad (10)$$

Since we have solutions (8) and (9), we can obtain $\mathrm{X_n}$ and v_n with (5b), (5e), and (5f) and then obtain u, v, and ϕ by using (2a) and (2b). We can also solve the horizontal divergence field with (1c): that is,

$$\frac{\partial u}{\partial x} + \frac{\partial v}{\partial y} = Q - \varepsilon\phi. \quad (11)$$

The q_n in (7) can be found by

$$q_n = \frac{1}{n!\sqrt{2\pi}} \int_{-\infty}^{\infty} A \exp[-\lambda^2(y - y_c)^2] D_n(y)\, dy. \quad (12)$$

Since, for $-6 < y_c < 6, \lambda = 1/2$, the values of q_n ($n = 7, 8, \ldots$) are much smaller than the minimum among the first seven q_n ($n = 0, 1, 2, \ldots, 6$), the response involving q_n up to order six is a good approximation. Finally we have the solutions of the atmospheric response to such a forcing, as shown below:

$$u = \frac{1}{2}\left\{\sum_{n=0}^{4} [\Psi_n D_n(y) - \mathrm{X_n} D_n(y)] + \sum_{n=5}^{6} \Psi_n D_n(y)\right\}, \quad (13a)$$

$$\phi = \frac{1}{2}\left\{\sum_{n=0}^{4} [\Psi_n D_n(y) + \mathrm{X_n} D_n(y)] + \sum_{n=5}^{6} \Psi_n D_n(y)\right\}, \quad (13b)$$

$$v = \sum_{n=0}^{5} v_n D_n(y), \quad (13c)$$

and

$$\frac{\partial u}{\partial x} + \frac{\partial v}{\partial y} = Q - \varepsilon\phi. \quad (13d)$$

Note that X_n ($n = 5$ and 6) and v_n ($n = 6$) are involved with q_n ($n = 7, 8, \ldots$) on the basis of the relationships described in (5b) and (5f); therefore, they are ignored in (13a)–(13c).

b. Model results

The model and forcing parameters are prescribed as $\varepsilon = 0.1$ and $\alpha = \lambda = 0.5$. The value of A is selected on the basis of the observations. A relatively weak anomalous heating source associated with the ASM is located over Australia centered around 25°S, 135°E and a strong anomalous cooling source associated with the EAWM is located over the Asian continent centered around 40°N, 115°E as seen in Fig. 1a. For such an idealized model, it is appropriate to choose the cooling center (−0.5, 4.0) and the heating center (1.5, −2.5) if the real location 0°, 120°E is taken to represent (0, 0) in the model. Three experiments are described and performed below.

1) Steady atmospheric response to an anomalous cooling over East Asia

The forcing for the first experiment (EXP1) is $Q(x, y) = 2.5 \exp[-\lambda^2(y - y_c)^2 - \alpha^2(x - x_c)^2]$, where $x_c = -0.5$ and $y_c = 4.0$: that is, the center of the Gaussian function $Q(x, y)$ is at (−0.5, 4.0), corresponding to about 40°N. Figure 5a shows this forcing.

Figure 5b shows the distribution of the anomalous horizontal divergence of low-level winds due to such an anomalous cooling. It is clear that the strong horizontal divergence is primarily located at the forcing region (i.e., the midlatitudes). The center of divergence (convergence) appears in the eastern (western) portion of the forcing as shown in Fig. 5b. Such a phenomenon can be simply explained by the off-equator vorticity equation, $\beta v + f\nabla \cdot \mathbf{V} = 0$. In the eastern (western) portion of anticyclonic circulation in the Northern Hemisphere ($f > 0$), $\beta v < 0$ ($\beta v > 0$), so $\nabla \cdot \mathbf{V} > 0$ ($\nabla \cdot \mathbf{V} < 0$); therefore, the horizontal divergence (convergence) occurs in the east (west) portion of the forcing. This distribution of the low-level divergence/convergence field is conducive to the formation of low pressure to the west of the forcing (cooling source). Figure 5b shows an anomalous low pressure located to the west of an anomalous high pressure.

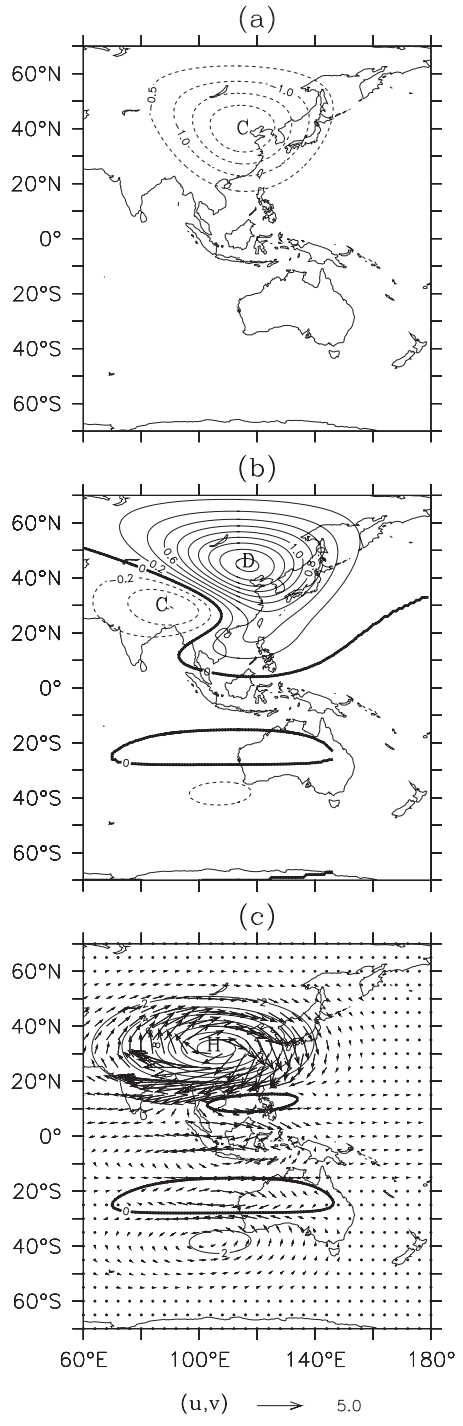

FIG. 5. (a) An ideal steady cooling source indicated by C with Gaussian distribution over the northeast Asian region. The signal of $Q(x, y)$ is reversed in this figure to be consistent with Fig. 1a. Contour interval is 0.5. (b) Distribution of anomalous, nondimensional, low-level horizontal divergence field. Contour interval is 0.2. The maximum horizontal divergence value is 1.4, indicated by D, and the maximum horizontal convergence value is −0.6, indicated by C. (c) Distribution of anomalous, nondimensional, low-level winds and geopotential height fields. Contour interval is 2.0. The maximum value is 16, indicated by H.

Figure 5c shows the distribution of the anomalous low-level winds and geopotential height. A strong anticyclonic circulation in the midlatitudes is formed. This anticyclonic circulation has a slight northeast–southwest tilt caused by the different roles that Rossby waves play in the midlatitudes and regions near the equator. In the midlatitudes, high-order Rossby waves have an important role; however, they primarily affect the adjacent regions of the forcing because of their small phase speed and rapid dissipation. In regions near the equator, low-order Rossby waves play a dominant role. Since low-order Rossby waves have relatively large amplitudes, fast phase speeds, and slow dissipation, their impact can extend to remote regions. There are strong northerly anomalies in the eastern portion of the anticyclonic circulation, similar to the observed anomalous northerly winds shown in Fig. 1b. Most importantly, weak westerly anomalies emerge near the WTP. This is because of the impact of Kelvin waves associated with the southwestward extension of the midlatitude cold high pressure system due to the northeast–southwest phase tilt. An eastward-propagating Kelvin wave develops when the midlatitude cold high pressure system extends southwestward to a region close to the equator, thus generating westerly anomalies. These weak westerly anomalies are mostly confined to a region 0°–10°N, 90°–140°E that differs from that in observations (Fig. 1b). Comparable easterly anomalies are mostly confined to 10°S–0°, 90°–140°E. This implies that the observed low-frequency westerly anomalies in boreal winters preceding the El Niño onset are probably not produced by the anomalous EAWM alone.

The simple model does not consider the dynamical effects of the Tibetan Plateau. For a realistic simulation, the dynamical effects because of the topography of the Tibetan Plateau would certainly be important in connecting the extratropics to the tropics and should not be ignored. For example, a large influx of surface cold surge from the very cold region of Siberia into central and southeast China can cause a rapid cooling of the lower troposphere and a rapid rise in surface pressure because of the Tibetan Plateau. Ultimately this cooling might produce a westerly anomaly over the WTP that would be different from a westerly anomaly produced without the effects of the Tibetan Plateau.

2) STEADY ATMOSPHERIC RESPONSE TO AN ANOMALOUS HEATING OVER AUSTRALIA

A second experiment (EXP2) is performed in which the atmosphere is forced only by a weak heating in Australia, expressed as $Q(x, y) = -1.5 \exp[-(y - y'_c)^2\lambda^2 - (x - x'_c)^2\alpha^2]$. The term on the right-hand side represents a heating source. Values of $y'_c = -2.5$ and $x'_c = 1.5$

represent a heating center located at about 25°S and a distance between the cooling and the heating sources of about 20° in longitude. Figure 6a shows the spatial distribution of the forcing and Fig. 6b reveals the anomalous low-level horizontal divergence field driven by such forcing. There is a strong convergence over Australia, along with a weak divergence just west of Australia (30°–20°S, 100°E). Figure 6c shows the distribution of anomalous low-level winds and geopotential height. A cyclonic circulation is found in the Southern Hemisphere in response to the heating over Australia. The weak tilt of this cyclonic circulation can be explained by Rossby wave arguments similar to those used to explain the tilt of anticyclones in the Northern Hemisphere. Southerly anomalies appear in the western portion of the cyclonic circulation.

Our model result reveals a weak low-level divergence to the west of the cyclone over Australia (Fig. 6b), which is conducive to the formation of such a high pressure. More importantly, the modeled westerly anomalies generated in the north of Australia (20°S–0°) are associated with the southerly anomalies in the western portion of the cyclonic circulation, which is consistent with the observation (Fig. 1b) that westerly anomalies found in the north of Australia (20°S–0°) are guided by the southerly anomalies in the west of Australia owing to the anomalous warming over Australia.

Certainly, there are discrepancies in the Southern Hemisphere in Figs. 1b and 6c. For example, there are westerly anomalies in the south of Australia in Fig. 1b that are replaced by easterly anomalies in Fig. 6c. Such discrepancies are expected because the forcing for the model is very simple and idealized, and in this study the model does not consider the cooling to the southwest of Australia in the Southern Hemisphere. It should be noted that, in addition to a contribution from the EAWM, as discussed in the previous subsection, the ASM can cause the strong westerly anomalies in a band region 10°S–5°N extending to 140°E (Fig. 6c), which is another important contribution to the enhanced westerly anomalies, as will be discussed in the next subsection.

3) Steady atmospheric response to an anomalous cooling and heating

To consider the impact of both the anomalous cooling over the East Asian continent and the anomalous heating over Australia, we perform a third experiment (EXP3) with a combined forcing specified as $Q(x,y) = 2.5\exp[-(y-y_c)^2\lambda^2 - (x-x_c)^2\alpha^2] - 1.5\exp[-(y-y'_c)^2\lambda^2 - (x-x'_c)^2\alpha^2]$. Figure 7a depicts the form of this forcing, whose spatial pattern is similar to the basic structure of observed surface air temperature in East Asia and Australia in Fig. 1a.

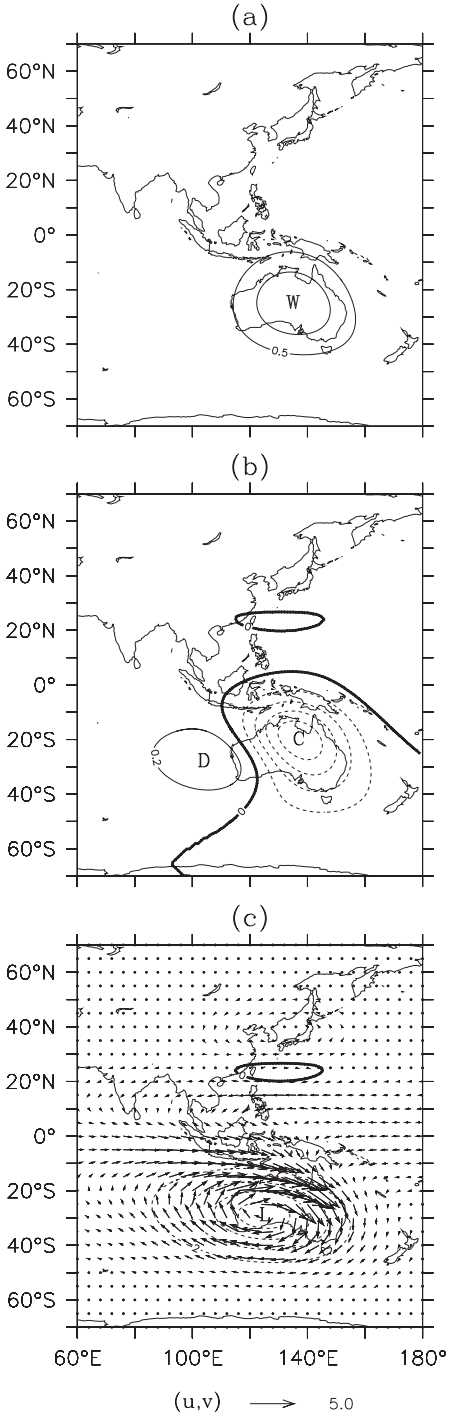

FIG. 6. As in Fig. 5, except for the forced heating over Australia. (a) An ideal steady warming source indicated by W with Gaussian distribution over Australia. Contour interval is 0.5. (b) Distribution of anomalous, nondimensional, low-level horizontal divergence field. Contour interval is 0.2. The maximum horizontal divergence value is 0.2, indicated by D, and the maximum horizontal convergence value is −1.0, indicated by C. (c) Distribution of anomalous, nondimensional, low-level winds and geopotential height fields. Contour interval is 2.0. The maximum value is −8.0, indicated by L.

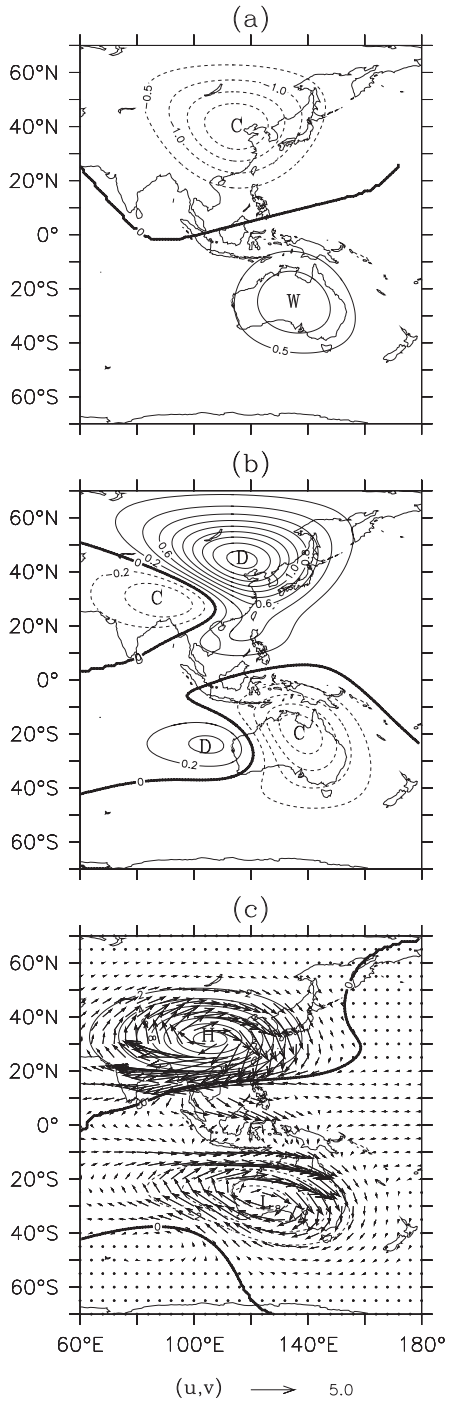

FIG. 7. As in Figs. 5 and 6, except for the simultaneous cooling over the northeast Asian region and heating over Australia. (a) Distribution of forcing. Contour interval is 0.5. (b) Distribution of anomalous, nondimensional, low-level horizontal divergence field. Contour interval is 0.2. In the Northern Hemisphere, the maximum horizontal divergence value is 1.4, indicated by D, and the minimum horizontal convergence value is −0.6, indicated by C. In the Southern Hemisphere, the maximum horizontal divergence value is 0.4 and the maximum horizontal convergence value is −1.0. (c) Distribution of anomalous, nondimensional, low-level winds and geopotential height fields. Contour interval is 2.0. The maximum value is 16.0, indicated by H, and the minimum value is −8.0, indicated by L.

TABLE 3. Strength of WA averaged over three regions in response to thermal forcing in three experiments.

Area-averaged WA region	EXP1 (cooling)	EXP2 (heating)	EXP3 (heating + cooling)
10°S–10°N, 110°–160°E	0.104	0.347	0.451
10°S–10°N, 110°–140°E	0.021	0.876	0.897
10°S–10°N, 140°–160°E	0.228	−0.448	−0.220

Figure 7b illustrates the spatial pattern of the horizontal divergence of the low-level winds in response to the simple forcing. Figure 7c depicts the anomalous low-level atmospheric circulation. The enhanced westerly anomalies near the WTP in response to the concurrent forcing over East Asia and Australia, the most relevant result, are reasonably consistent with the observations (Fig. 1b). For example, pronounced westerly anomalies are present between 10°S–10°N and 90°–140°E. The enhanced westerly anomalies over the WTP is due to the convergence of westerly anomalies in the northern portion of the cyclonic circulation associated with ASM in the Southern Hemisphere with the westerly anomalies generated by Kelvin waves associated with the cold high pressure system over the Siberia–Mongolia region closely tied to a strong EAWM. The area-averaged westerly anomalies are computed over three regions, 10°S–10°N, 110°–160°E; 10°S–10°N, 110°–140°E; and 10°S–10°N, 140°–160°E, for these three experiments, and the results are listed in Table 3. Table 3 clearly shows that the westerly anomalies over regions 10°S–10°N, 110°–160°E and 10°S–10°N, 110°–140°E are significantly enhanced if anomalous heating over Australia associated with the ASM is added to the total thermal forcing. The reason for westerly (easterly) anomalies in 10°S–10°N, 140°–160°E appearing to the east of the cooling (heating) region has been explained by Gill (1980). The westerly anomalies in 10°S–10°N, 140°–160°E resulting from cooling in East Asia (Fig. 5c) are completely offset by the stronger easterly anomalies resulting from heating in Australia (Fig. 6c) because the heating region is much closer to the equator than the cooling region is. As a consequence, the model simultaneously produces the weak easterly anomalies in 10°S–10°N, 140°–160°E in response to the cooling in East Asia and heating in Australia (Fig. 7c). This explains why the confluent westerly anomalies are concentrated in the Indonesian Maritime Continent region (i.e., west of 140°E) in the model. It is worth noting that the area-averaged westerly anomaly due to the EAWM alone in 10°S–10°N, 110°–140°E (EXP1; Table 3) is much smaller than the anomaly in 10°S–10°N, 140°–160°E because the westerly anomalies in 0°–10°N, 110°–140°E are strongly offset by the comparable easterly anomalies in 10°S–0°,

110°–140°E (Fig. 5c). Nevertheless, the observational result that the anomalous EAWM and ASM concurrently enhance westerly anomalies over the WTP is probably associated with the atmospheric response to a combined anomalous thermal forcing over Siberia–Mongolia and Australia, which is evident in our simple model. The nondimensional values in Table 3 are comparable to the observations if a reasonable dimension scale is given; thus, the westerly anomalies over the WTP forced with the EAWM and the ASM in the model are not trivial. For example, for a tropical atmosphere with an equivalent depth of 400 m, the length scale (i.e., Rossby deformation radius) is about 1000 km, and if the anomalous 6-month-averaged heating rates (dT/dt) associated with the EAWM and the ASM are assumed to be $-0.5\,\mathrm{K\,day^{-1}}$ ($\sim -15\,\mathrm{W\,m^{-2}}$) and $0.3\,\mathrm{K\,day^{-1}}$ ($\sim 9\,\mathrm{W\,m^{-2}}$), respectively, then an area-averaged, nondimensional westerly anomaly of 0.451 (Table 3) is equivalent to a dimensional value of about $0.3\,\mathrm{m\,s^{-1}}$, which is comparable to the observed $0.33\,\mathrm{m\,s^{-1}}$ (Fig. 3d) computed from the NCEP–NCAR Reanalysis 1 product.

5. Effect of mean zonal wind on westerly anomalies over the WTP

In section 4, the analytical solutions are based on the rest atmosphere. If the mean state is taken into account, how does the atmosphere respond to the diabatic heating? If a basic state with constant zonal wind U is included in the shallow-water equations of (1a)–(1c), the analytical solutions (8) and (9) are then given by

$$\Psi_0 = q_0 \exp[-\varepsilon(x-x_c)/(U+1)]\delta_0 \frac{\sqrt{\pi}\exp\left[\dfrac{\varepsilon}{2\alpha(U+1)}\right]^2}{2\alpha(U+1)} \times \mathrm{Erfc}\left\{\delta_0\left[\frac{\varepsilon}{2\alpha(U+1)} - \alpha(x-x_c)\right]\right\} \tag{14}$$

and

$$\Psi_{n+1} = (nq_{n+1} + q_{n-1})\exp\left[-\frac{\varepsilon(x-x_c)}{U-c_n}\right]\delta_n \times \frac{\sqrt{\pi}\exp\left[\dfrac{\varepsilon}{2\alpha(U-c_n)}\right]^2}{2\alpha(2n+1)(U-c_n)} \times \mathrm{Erfc}\left\{\delta_n\left[\alpha(x-x_c) - \frac{\varepsilon}{2\alpha(U-c_n)}\right]\right\}, \tag{15}$$

respectively, where $\delta_0 = 1$ (-1) if the sign of $U + 1$ is positive (negative); $\delta_n = 1$ (-1) if the sign of $U - c_n$ is positive (negative). If $U + 1 = 0$ or $U = c_n$ (i.e., at the stationary resonant condition), the solutions of (14) and (15) become indeterminate. In this case, using the asymptotic expansion

$$\mathrm{Erfc}(t) \sim (\sqrt{\pi}t)^{-1}\exp(-t^2), \tag{16}$$

the solutions are estimated by

$$\Psi_0 = \frac{1}{\varepsilon}q_0\exp[-\alpha^2(x-x_c)^2] \tag{17}$$

and

$$\Psi_{n+1} = \frac{1}{\varepsilon}\frac{nq_{n+1}+q_{n-1}}{2n+1}\exp[-\alpha^2(x-x_c)^2]. \tag{18}$$

The three experiments discussed in section 4 are conducted again to illustrate the atmospheric steady response but with a basic zonal wind, $U = -0.1$ and $U = 0.1$ representing the easterly and westerly regimes, respectively. Figure 8 shows the effect of the mean zonal wind on the anomalous low-level winds and geopotential height fields, in contrast to a rest atmosphere. The longitudinal Doppler-shifted atmospheric circulation is evident because of a mean zonal wind: that is, the entire atmospheric circulation shifts westward (eastward) in the westerly (easterly) regime. In addition, the zonal asymmetry in the easterly regime is more apparent than that in the westerly regime. For example, the Rossby waves to the west of forcing in the easterly regime propagate farther downstream with an elongated circulation (Fig. 8a) than those in the westerly regime (Fig. 8c). Interestingly, the major atmospheric circulation extends farther in the zonal direction in the easterly regime because the atmosphere extends farther toward the equator in the easterly regime in both the Northern and Southern Hemispheres. These changes to the atmospheric circulation owing to the mean zonal wind modulate the westerly anomalies over the WTP (110°–160°E), which are summarized in Table 4. Although the westerly anomalies over the WTP due to the EAWM are not sensitive to changes of mean zonal wind, they are sensitive to changes of mean zonal wind through the ASM. Overall, the westerly regime favors stronger westerly anomalies over the WTP, primarily from a contribution of strong confluent flow in the north of Australia within the ASM system, which causes a larger westerly anomaly than that reduced by the EAWM. Here we emphasize that the enhancement of the westerly anomalies over the WTP is still caused by the co-impact of the EAWM and the ASM, regardless of the effect of a mean zonal wind.

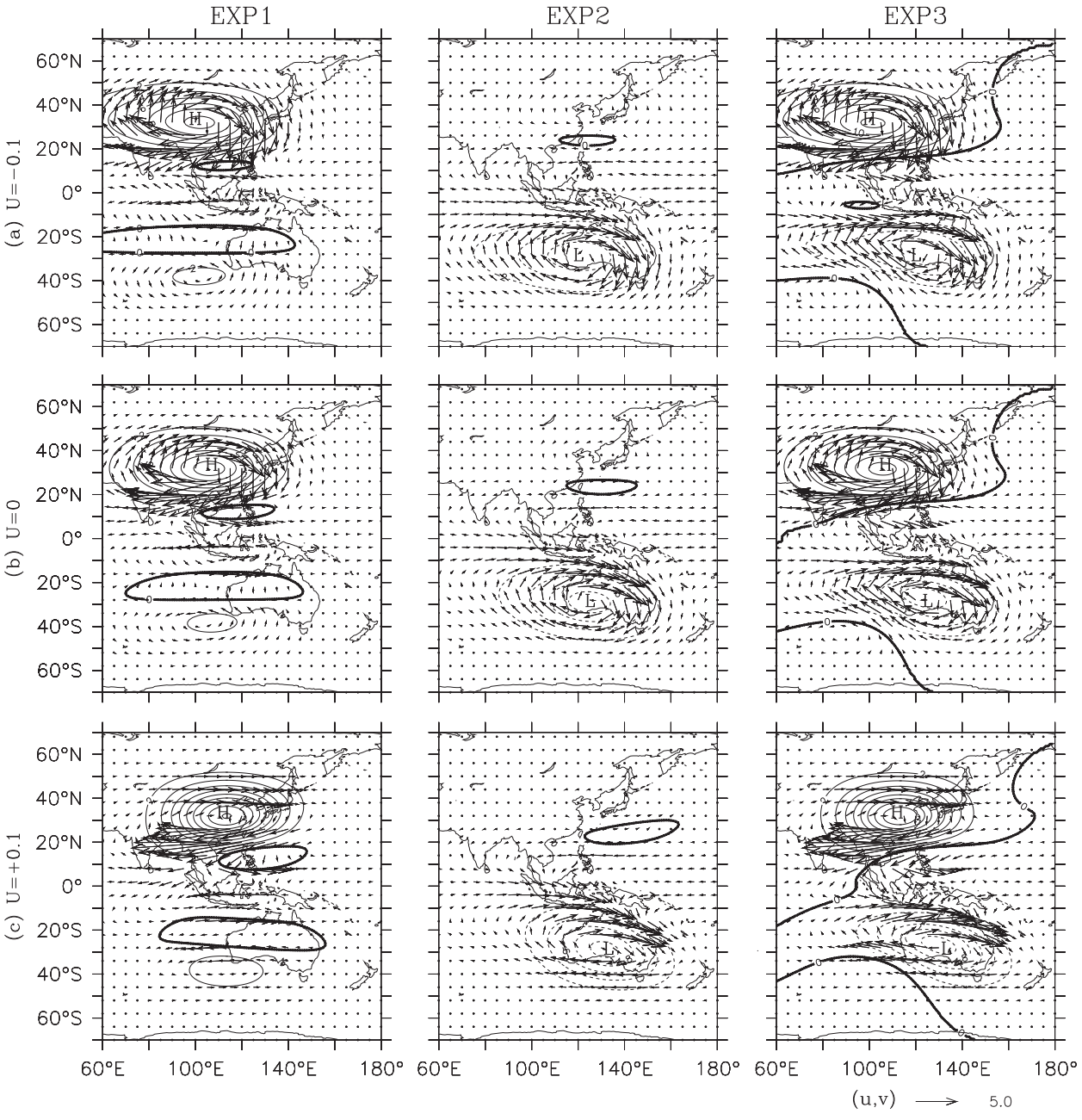

FIG. 8. Distributions of anomalous low-level winds (vectors) and geopotential height fields (contours) from three experiments, (left) EXP1, (center) EXP2, and (right) EXP3, in (a) $U = -0.1$, (b) $U = 0$, and (c) $U = +0.1$. Contour interval is 2.0. The locations of maximum and minimum values are indicated by H and L, respectively. The thermal forcing is the same as in (a) of Figs. 5–7.

In reality, the influence of the mean zonal wind on the westerly anomalies over the WTP is expected to be more complicated because of other factors such as horizontal wind shear, which would alter the properties of the equatorial modes (e.g., Boyd 1978). However, if we concentrate on the WTP region where the local mean state wind shear is tiny, the simple experiments may provide a clue that the observed westerly anomalies can be strengthened by a strong anomalous EAWM and a strong ASM.

6. Discussion and conclusions

Our simple model experiments show that when anomalous northerlies from the boreal winter EAWM converge with anomalous southerlies from the boreal

TABLE 4. Strength of WA averaged over the region 10°S–10°N, 110°–160°E in response to thermal forcing in three experiments for the easterly and westerly regimes, compared with a rest atmosphere.

Area-averaged WA regime	EXP1 (cooling)	EXP2 (heating)	EXP3 (heating + cooling)
$U = -0.1$ (easterly)	0.105	0.222	0.327
$U = 0$ (rest atmosphere)	0.104	0.347	0.451
$U = 0.1$ (westerly)	0.090	0.519	0.609

summer ASM, westerly anomalies over the WTP are enhanced as a result of the Kelvin wave response. We conclude that the model captures the basic features of atmospheric circulation (Figs. 7b,c) on the basis of comparison to the observations shown in Fig. 1b. The simulated westerly anomalies over the WTP forced with the EAWM and the ASM in the model are not trivial when compared to the observations. If a constant mean zonal wind is considered in the model, it primarily produces a longitudinal Doppler shift circulation relative to a rest atmosphere (Fig. 8b), giving rise to a change in the westerly anomalies over the WTP. Westerly anomalies over the WTP can be enhanced by the co-impact of a strong anomalous EAWM and a strong ASM, regardless of a mean state of atmosphere.

However, the shortcomings of this simple model are also obvious. For example, in our model the low-level horizontal divergence (convergence) field in the Northern Hemisphere (Southern Hemisphere) is stronger than the low-level convergence (divergence) field to its west. This is not the case in the observations (Fig. 1b). The discrepancies between the model and the observations are partly as a result of the simple forcing. The model does well in reproducing westerly anomalies over the WTP, except for the region (0°–10°S), where the westerly anomalies in this model are mostly constrained to the west of 140°E (i.e., over Indonesia and northern Australia), whereas the observed westerly anomalies over the WTP can typically reach 160°E, as shown in Fig. 1b. This difference probably happens because the anomalous southerlies off the northeastern coast of Australia (Xu and Chan 2001; Zhang et al. 2001), which are related to the anomalous cyclones over the South Pacific convergence zone as discussed by Xu and Chan (2001), are missing in this simple model. Nonetheless, the simple model captures some of the observed fundamental features. The difference in the model's atmospheric features should be expected because of the shortcomings described above. In addition, the observed westerly anomalies over the WTP for some individual years after 1990 (Figs. 2, 3) do not exactly reflect the co-impact of the EAWM and the ASM on the amplitude of the westerly anomalies as shown in the model (Figs. 5–7). Such discrepancy in the generation of the westerly anomalies over the WTP between the model and the observations implies that nonlinearity as well as mechanisms other than the monsoons may influence the generation of anomalous westerlies over the WTP. The weaker EAWM (i.e., southerly anomalies) after 1990 may be attributed to the decadal shift of the EAWM because the winters in East Asia become much warmer after 1990 (Wang et al. 2009), also seen in this study (Fig. 4a). Previous studies indicated that WP El Niño events with major SSTA centered in the central Pacific Ocean near the edge of the warm pool mostly occurred after 1990; CT El Niño events with SSTA positioned in the eastern Pacific Ocean mostly occurred before 1990. The advent of a weak EAWM after 1990 may be associated with the change of El Niño type from CT to WP.

This study uses only the prescribed localized steady heat sources to drive the atmosphere; these extratropical diabatic heating/cooling sources may last several months, much longer than the 30–60-day MJO period. Therefore, the temporal variability of westerly anomalies and their connection to the MJO are excluded. A recent study showed that low-frequency (more than 90 days but less than 6 months) surface winds play a major role in El Niño events, and high-frequency (<90 days) surface winds may modulate their amplitudes (Rong et al. 2011). This study's result suggests that low-frequency WTP surface westerly anomalies relevant to El Niño onset may be produced by the combination of anomalous EAWM and ASM systems. It should be noted that the forcing is simple and the ratio of cooling amplitude over the Siberia–Mongolia region to heating amplitude over Australia is roughly set according to the composite analysis. Therefore, the model results may be suitable for qualitative discussion but not for explaining an individual case. Furthermore, the model does not consider the effects of the Tibetan Plateau, which would certainly be important in realistic atmospheric simulations. The model is also limited because of lack of nonlinearity; however, the impact of nonlinearity is beyond the scope of the present study.

This study is focused on the influence of the EAWM and the ASM on low-frequency westerly anomalies over the WTP. However, the EAWM and the ASM may be modulated by the tropical convection associated with westerly anomalies over the WTP. For example, the EAWM can be affected by ENSO through a change of convection over the tropical western Pacific Ocean (e.g., Zhang et al. 1996). Other previous studies (e.g., Sakai and Kawamura 2009; Hendon and Liebmann 1990) indicated that tropical convection associated with westerly anomalies over the WTP may play a role in the onset

and development of the EAWM and the ASM. The feedback of tropical convective anomalies associated with the WTP's westerly anomalies, which is beyond the scope of this study, deserves further discussion in a future study.

Finally, the model and forcing in this study are not constructed specifically for the study of El Niño episodes. The observational features of an anomalous, cold, high pressure system over the Siberia–Mongolia region and an anomalous, warm, low pressure system over Australia in boreal winters are associated with the EAWM and the ASM preceding the onset of El Niño. Therefore, the reproduction of westerly anomalies in this model is an attempt to explain the generation of enhanced surface westerlies associated only with the anomalous EAWM and ASM.

Acknowledgments. We are greatly indebted to those who contributed to the observational datasets used in this study. Comments from two anonymous reviewers have improved the overall quality of this paper. Computational facilities were provided by the Center for Ocean–Atmospheric Prediction Studies (COAPS), the Florida State University. Yangxing Zheng was supported by U.S. National Science Foundation (NSF) Grant OCE-0453046, AGS 0966844, and the National Aeronautics and Space Administration (NASA) Physical Oceanography support of the Ocean Vector Winds Science Team (OVWST). Renhe Zhang was supported by the National Natural Science Foundation of China under Grant 41221064 and the Special Scientific Research Project of China Commonweal Trade (meteorology) under Grant GYHY201306018. Mark Bourassa was supported by the NASA OVWST and NOAA Climate Observing Division (COD).

REFERENCES

Ashok, K., S. K. Behera, S. A. Rao, H. Weng, and T. Yamagata, 2007: El Niño Modoki and its possible teleconnection. *J. Geophys. Res.,* **112,** C11007, doi:10.1029/2006JC003798.

Battisti, D. S., 1988: Dynamics and thermodynamics of a warming event in a coupled tropical atmosphere–ocean model. *J. Atmos. Sci.,* **45,** 2889–2919.

——, and A. C. Hirst, 1989: Interannual variability in a tropical atmosphere–ocean model: Influence of the basic state, ocean geometry and nonlinearity. *J. Atmos. Sci.,* **46,** 1687–1712.

Boyd, J. P., 1978: The effects of latitudinal shear on equatorial waves. Part II: Application to the atmosphere. *J. Atmos. Sci.,* **35,** 2295–2267.

Cane, M. A., and S. E. Zebiak, 1985: A theory for El Niño and the Southern Oscillation. *Science,* **228,** 1084–1087.

——, ——, and S. C. Dolan, 1986: Experimental forecasts of El Niño. *Nature,* **321,** 827–832.

Chu, P. S., 1988: Extratropical forcing and the burst of equatorial westerlies in the western Pacific: A synoptic study. *J. Meteor. Soc. Japan,* **66,** 549–563.

Compo, G. P., G. N. Kiladis, and P. J. Webster, 1999: The horizontal and vertical structure of East Asian winter monsoon pressure surges. *Quart. J. Roy. Meteor. Soc.,* **125,** 29–54.

Gill, A. E., 1980: Some simple solutions for heat-induced tropical circulation. *Quart. J. Roy. Meteor. Soc.,* **106,** 447–462.

Gutzler, D. S., 1991: Interannual fluctuations of intraseasonal variance of near-equatorial zonal winds. *J. Geophys. Res.,* **96** (S01), 3172–3185.

Harrison, D. E., and G. A. Vecchi, 1997: Westerly wind events in the tropical Pacific, 1986–95. *J. Climate,* **10,** 3131–3156.

Hendon, H. H., and H. B. Liebmann, 1990: A composite study of onset of the Australian summer monsoon. *J. Atmos. Sci.,* **47,** 2227–2240.

——, and ——, 1994: Organization of convection within the Madden-Julian oscillation. *J. Geophys. Res.,* **99** (D4), 8073–8083.

——, ——, and J. D. Glick, 1998: Oceanic Kelvin waves and the Madden–Julian oscillation. *J. Atmos. Sci.,* **55,** 88–101.

Huang, R., X. Zang, R. Zhang, and J. Chen, 1998: The westerly anomalies over the tropical Pacific and their dynamical effect on the ENSO cycles during 1980-1994. *Adv. Atmos. Sci.,* **15,** 135–151.

Kalnay, E., and Coauthors, 1996: The NCEP/NCAR 40-Year Reanalysis Project. *Bull. Amer. Meteor. Soc.,* **77,** 437–471.

Kao, H.-Y., and J.-Y. Yu, 2009: Contrasting eastern-Pacific and central-Pacific types ENSO. *J. Climate,* **22,** 615–632.

Keen, R. A., 1982: The role of cross-equatorial tropical cyclone pairs in the Southern Oscillation. *Mon. Wea. Rev.,* **110,** 1405–1416.

——, 1988: Equatorial westerly and the Southern Oscillation. *Proc. Western Pacific Air-Sea Interaction Workshop,* Honolulu, HI, U.S. TOGA, 121–140.

Kiladis, G. N., and H. V. Loon, 1988: The Southern Oscillation. Part VII: Meteorological anomalies over the Indian and Pacific sectors associated with the extremes of the oscillation. *Mon. Wea. Rev.,* **116,** 120–136.

——, G. A. Meehl, and K. M. Weickmann, 1994: Large-scale circulation associated with westerly wind bursts and deep convection over the western equatorial Pacific. *J. Geophys. Res.,* **99** (D9), 18 527–18 544.

Kug, J.-S., F.-F. Jin, and S.-I. An, 2009: Two types of El Niño events: Cold tongue El Niño and warm pool El Niño. *J. Climate,* **22,** 1499–1515.

Larkin, N. K., and D. E. Harrison, 2005a: On the definition of El Niño and associated seasonal average U.S. weather anomalies. *Geophys. Res. Lett.,* **32,** L13705, doi:10.1029/2005GL022738.

——, and ——, 2005b: Global seasonal temperature and precipitation anomalies during El Niño autumn and winter. *Geophys. Res. Lett.,* **32,** L16705, doi:10.1029/2005GL022860.

Lau, K. M., and H. Lim, 1982: Thermally driven motions in an equatorial β-plane: Hadley and Walker circulations during the winter monsoon. *Mon. Wea. Rev.,* **110,** 336–353.

——, M. L. Peng, C. H. Sui, and T. Nakazawa, 1989: Super cloud clusters, westerly wind burst, 30–60 day oscillation, and ENSO: A unified view. *J. Meteor. Soc. Japan,* **67,** 205–219.

Li, C., 1990: Interaction between anomalous winter monsoon in East Asia and El Niño events. *Adv. Atmos. Sci.,* **7,** 36–46.

Lim, H., and C. P. Chang, 1981: A theory for midlatitude forcing of tropical motions during winter monsoons. *J. Atmos. Sci.,* **38,** 2377–2392.

Love, G., 1985a: Cross-equatorial influence of winter hemisphere subtropical cold surges. *Mon. Wea. Rev.,* **113,** 1487–1498.

——, 1985b: Cross-equatorial interactions during tropical cyclongenesis. *Mon. Wea. Rev.,* **113,** 1499–1509.

Matsuno, T., 1966: Quasi-geostrophic motions in the equatorial area. *J. Meteor. Soc. Japan,* **44,** 25–43.

Rasmusson, E. M., and T. H. Carpenter, 1982: Variations in tropical sea surface temperature and surface wind fields associated with the Southern Oscillation and El Niño. *Mon. Wea. Rev.,* **110,** 354–384.

Rong, X., R. Zhang, T. Li, and J. Su, 2011: Upscale feedback of high-frequency winds to ENSO. *Quart. J. Roy. Meteor. Soc.,* **137,** 894–907.

Sakai, K., and R. Kawamura, 2009: Remote response of the East Asian winter monsoon to tropical forcing related to El Niño–Southern Oscillation. *J. Geophys. Res.,* **114,** D06105, doi:10.1029/2008JD010824.

Smith, T. M., R. W. Reynolds, T. C. Peterson, and J. Lawrimore, 2008: Improvements to NOAA's historical merged land–ocean surface temperature analysis (1880–2006). *J. Climate,* **21,** 2283–2296.

Sui, C. H., and K. M. Lau, 1992: Multi-scale phenomena in the tropical atmosphere over the western Pacific. *Mon. Wea. Rev.,* **120,** 407–430.

Verbickas, S., 1998: Westerly wind bursts in the tropical Pacific. *Weather,* **53,** 282–284.

Wang, L., R. Huang, L. Gu, W. Chen, and L. Kang, 2009: Interdecadal variations of the East Asian winter monsoon and their association with quasi-stationary planetary wave activity. *J. Climate,* **22,** 4860–4872.

Webster, P. J., 1987: The elementary monsoon. *Monsoons,* J. S. Fein and P. L. Stephens, Eds., Wiley Interscience, 3–32.

Xu, J., and J. C. L. Chan, 2001: The role of the Asian–Australian monsoon system in the onset time of El Niño events. *J. Climate,* **14,** 418–433.

Xue, Y., T. Smith, and R. W. Reynolds, 2003: Interdecadal changes of 30-yr SST normals during 1871–2000. *J. Climate,* **16,** 1601–1612.

Yu, L., and M. M. Rienecher, 1998: Evidence of an extropical atmospheric influence during the onset of the 1997-98 El Niño. *Geophys. Res. Lett.,* **25,** 3537–3540.

Zhang, R., and R. Huang, 1998: The dynamic impacts of tropical zonal wind stress in the onset and decay of El Niño events. Part I: Data diagnostics and theoretic analysis. *Chin. J. Atmos. Sci.,* **22,** 587–599.

——, A. Sumi, and M. Kimoto, 1996: Impact of El Niño on the East Asian monsoon: A diagnostic study of the '86/87 and '91/92 events. *J. Meteor. Soc. Japan,* **74,** 49–62.

——, G. Zhao, and Y. Tan, 2001: Meridional wind stress anomalies over tropical Pacific and the onset of El Niño. Part I: Data analysis. *Adv. Atmos. Sci.,* **18,** 467–480.